PROCEEDINGS OF SPIE

Solid State Lasers and Amplifiers IV, and High-Power Lasers

Thomas Graf
Jacob I. Mackenzie
Helena Jelinková
Gerhard G. Paulus
Vincent Bagnoud
Catherine Le Blanc
Editors

12–16 April 2010
Brussels, Belgium

SPIE Photonics Europe

Sponsored by
SPIE

Cosponsored by
B-PHOT—Brussels Photonics Team (Belgium)
Brussels-Capital Region (Belgium)
FWO—Fonds Wetenschappelijk Onderzoek (Belgium)
ICO—International Commission for Optics
Ville de Bruxelles (Belgium)

Volume 7721

SPIE

High gain solid-state modules for picosecond pulses amplification

A. Agnesi, F. Pirzio*, G. Reali
INFN Sez. di Pavia and Electronics Dept. University of Pavia, Via Ferrata 1 - 27100 Pavia (Italy)

ABSTRACT

We present both numerical models and experimental results of ultra-short pulses solid-state laser grazing-incidence amplifier modules for generation of intense picosecond pulses, in various regimes from single shot to repetition rates of GHz.

Keywords: Solid State Lasers, Amplifiers, Ultra-short laser pulses

1. INTRODUCTION

Few picosecond mode-locked and sub-nanosecond passively Q-switched laser sources are becoming increasingly attractive for many industrial and scientific applications such as precision material processing[1,2], nonlinear optics[3,4] and laser spectroscopy[5]. In case of mode-locked picosecond sources, semiconductor saturable absorber mirrors (SESAMs) are widely employed devices[6]. SESAMs are very effective and highly reliable when used in low-power oscillators, however they require special design as their thermal management becomes very important when employed in high-power oscillators[7]. Indeed, the intense intracavity radiation of this particular operating regime may induce significant optical and thermo-mechanic stress effects, leading to rapid degradation. An alternative solution is the widely employed Master Oscillator Power Amplifier (MOPA). Grazing-incidence side-pumped Nd:YVO_4 slabs allow efficient power extraction owing to the very high single-pass gain achievable in such configuration[8,9] and offer excellent beam quality preservation owing to the total reflection leading to left-right inversion. Starting from robust, low-power diode-pumped solid-state oscillators, using programmable pulse-pickers one can select either a single pulse or a properly shaped pulse train for further amplification and compensation of envelope distortions due to gain saturation. This technology allows the realisation of compact, efficient and modular amplifiers, significantly simpler than, for example, cavity-based regenerative schemes.

Using quasi-cw (qcw) diode arrays as the pump source of Nd:YVO_4 slab amplifier, starting from ≈ 1 nJ, 10-ps pulse seed, amplified pulse energy as high as 200 μJ at 1 kHz can be obtained. Efficient harmonic and travelling-wave parametric generation are readily achieved with such high pulse peak powers.

When multi-MHz picosecond pulses or multi-kHz sub-nanosecond pulses are required, cw diode arrays are chosen as pump sources for the slab amplifiers. An 8-W, 8-ps laser system has been demonstrated starting from a 50-mW cw oscillator, at 150 MHz. When pulsewdiths of few hundreds picosecond can be considered, an even simpler architecture is especially attractive, starting from passively Q-switched (PQS) sub-nanosecond miniature (or monolithic) oscillators: a 577-ps multi-kHz laser system in a MOPA configuration, with a maximum average output power of 5.45 W and a peak power ≈ 1 MW at 10 kHz, in a diffraction- limited, single-axial frequency beam has been demonstrated recently. Owing to the effective gain shaping of the tightly pumped amplifier, no significant thermal distortion were detected, allowing nearly diffraction limited operation. Although high power picosecond oscillators have been demonstrated lately, these results are interesting since they suggest an alternative way for power-scaling of picosecond sources without pushing delicate intracavity components (such as SESAMs) to the damage limit.

Some other applications require instead the amplification of pulse trains, which can be conveniently extracted and amplified from a low-power oscillator at the desired repetition rate. For example, starting from a 20-mW, 5-GHz picosecond oscillator we amplified trains of few thousands of pulses up to 2 mJ with three slab amplifiers (as much as 300 mJ were achieved with two additional Nd:YAG flash-lamp-pumped post-amplifiers). Such pulse trains are very effective for synchronous pumping of optical parametric oscillators, lowering significantly their threshold with respect to the travelling-wave geometry.

*federico.pirzio@unipv.it; phone +39 0382 985-225; fax +39 0382 422-583;

Solid State Lasers and Amplifiers IV, and High-Power Lasers, edited by Thomas Graf, Jacob I. Mackenzie, Helena Jelinková, Gerhard G. Paulus, Vincent Bagnoud, Catherine Le Blanc, Proc. Of SPIE Vol. 7721, 77210C · © 2010 SPIE · CCC code: 0277-786X/10/$18 · doi: 10.1117/12.859055

2. NUMERICAL MODEL

2.1 Operation in CW regime

The model is based on standard cw amplifier theory[10]. A useful reference system for the beam propagation is defined in Fig. 1. The length and the thickness of the slab are L and W, respectively.

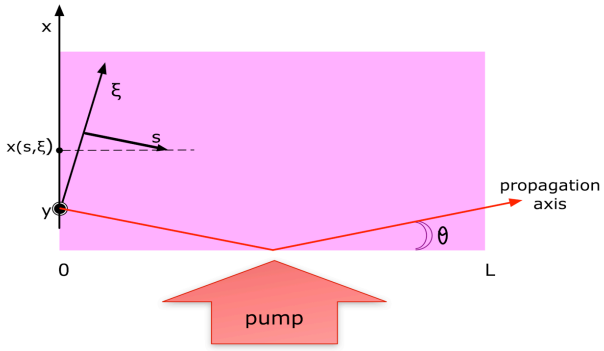

Figure 1. Model of the slab amplifier (seen from above): the beam enters from the left side with a grazing angle θ. The beam cross section is most easily described by coordinates (ξ,y).

In particular, the transverse reference frame for the seed beam is ξ–y. Assuming small grazing angles, i.e. $\theta << 1$ rad, we may approximate $x(s,\xi) = \theta L/2 + \xi - s\theta$. In order to optimize the overlap efficiency, propagation inside the amplifier has to occur with a nearly-constant beam cross section, therefore the gain can be calculated along the longitudinal s coordinate as in a ray-tracing approximation:

$$\frac{dI(\xi,y)}{ds} = \sigma n(x,y) I(\xi,y) \tag{1}$$

The saturated population inversion density is

$$n(x,y) = \frac{R_P(x,y)\tau}{1 + I(\xi,y)/I_S} \tag{2}$$

and the pump rate is given by

$$R_P(x,y) = \frac{\lambda_P}{\lambda_L}\frac{\alpha_p}{WL}\frac{P_{inc}\,\Theta(y)\,e^{-\alpha_P x}}{h\nu} \tag{3}$$

The step function Θ is defined as: $\Theta(y) = 1$ for $|y| < W/2$, $\Theta(y) = 0$ for $|y| > W/2$; σ is the stimulated emission cross section at the laser frequency $\nu = c / \lambda_L$; τ is the fluorescence time; $I_s = h\nu / (\sigma\tau)$ is the laser saturation intensity; α_P is the saturated absorption coefficient at the pump wavelength λ_P, corresponding to the incident pump intensity $I_P = P_{inc} / (WL)$ (P_{inc} is the power transmitted through the pump face and absorbed by the crystal), $\alpha_P = \alpha_{P0} / (1 + I_P / I_{SP})$ and I_{SP} is the pump absorption saturation intensity[11]. Inserting Eqs. (2) and (3) into Eq. (1) and integrating, one obtains

$$\ln\left[\frac{I_o(\xi,y)}{I_i(\xi,y)}\right] + \frac{I_o(\xi,y) - I_i(\xi,y)}{I_S} = \frac{\lambda_P}{\lambda_L}\frac{\alpha_P P_{inc}\Theta(y)}{WLI_S}\int_0^L ds\exp\left[-\alpha_P\left|x(\xi,s)\right|\right] \tag{4}$$

Imposing that the forward-traveling intensity equals the backward-traveling intensity at $s = L$, a double-pass model can be readily derived from Eqs. (1-3). We assume that, after the first pass, the beam retraces its path backward through the amplifier. Eventually, we end up with two equations, one for the single-pass (q = 1) and one for the double-pass amplifier (q = 1/2):

$$q \ln\left[\frac{I_o(\xi,y)}{I_i(\xi,y)}\right] + \frac{I_o(\xi,y) - I_i(\xi,y)}{I_S} = \frac{\lambda_P}{\lambda_L}\frac{\alpha_P P_{inc}\Theta(y)}{WLI_S}\psi(\xi) \tag{5}$$

where

$$\psi(\xi) = \frac{2}{\alpha_P\theta}\left[1 - \cosh(\alpha_P\xi)\exp\left(-\frac{\alpha_P\theta L}{2}\right)\right] \tag{6}$$

Notice that the small-signal gain coefficient is proportional to the right-hand side of Eq. (5): it is assumed to have a flat-top profile in the vertical direction while it has a smooth symmetric profile in the horizontal ξ-direction, with a peak on axis. This is a consequence of the bounce occurring at the mid-point of the slab. Moreover, thermal distortions that usually accompany the pump deposition are averaged accordingly, yielding the same symmetry as for the gain distribution along the ξ axis. Thermal lensing retains the usual distribution along the y axis. As anticipated, an arbitrary seed beam profile can now be traced along the amplifier with Eqs. (5) and (6).

A particularly handy approximation, that speeds up the calculations significantly, consists in assuming an average gain coefficient over the horizontal seed diameter:

$$\bar{\psi} = \frac{2}{w_s}\int_0^{w_s/2}\psi(\xi)\,d\xi = \frac{2}{\alpha_P\theta}\left[1 - \frac{2}{\alpha_P w_s}\sinh(\alpha_P w_s/2)\exp\left(-\alpha_P\theta L/2\right)\right] \tag{7}$$

Rather than the transverse intensity distribution of the rays with coordinates (ξ,y), the spatially-averaged Eq. (5) yields now a single output intensity, given the seed cross section $w_s \times W$ and the input intensity:

$$q \ln\left[\frac{I_o}{I_i}\right] + \frac{I_o - I_i}{I_S} = \frac{\lambda_P}{\lambda_L}\frac{\alpha_P P_{inc}}{WLI_S}\bar{\psi} \tag{8}$$

It is worth noticing that the crystal end faces limit the effective width of the input seed. The beam width may be comparable with the distance between the centre of the beam and the edge of the slab input face, i.e. $\theta L/2$. On the other hand, when increasing the angle θ there is a possibility that the beam width becomes comparable with its distance from the other edge of the slab, of width D. Therefore, the effective beam diameter to be amplified is the minimum out of the quantities w_s, θL and $2(D\text{-}\theta L/2)$.

2.2 Amplification in pulsed, low-frequency regime ($f << 1/\tau$)

In pulsed amplification regime, usually a pulse-picker selects a single pulse from a cw mode-locked laser and sends it to the amplifier that was previously pumped to achieve an appropriate gain level. Assuming pump pulse duration T, and averaging the spatial gain distribution as in Eq. (7), the pump rate equation yields the small-signal exponential gain:

$$\frac{dn}{dt} = R_P - \frac{n}{\tau} \tag{9}$$

$$g_0 = \left\langle \int_0^L \sigma n\,ds \right\rangle = \frac{2}{w_s}\int_0^{w_s/2} d\xi\left[\int_0^L \sigma n(\xi,s)\,ds\right] = \sigma R_P \tau\left(1 - e^{-T/\tau}\right)\bar{\psi} \tag{10}$$

$$g_0 = \frac{\lambda_P}{\lambda_L}\frac{E_{inc}}{WLF_S}\frac{\tau}{T}\left(1 - e^{-T/\tau}\right)\alpha_P\bar{\psi} \tag{11}$$

We may now use the Franz-Nodvik amplifier model[12] to calculate the output fluence F_o, given the input fluence F_i and the amplifier saturation fluence $F_S = h\nu/\sigma$:

$$F_o = F_S \ln\left[1 + e^{g_0}\left(e^{F_i/F_S} - 1\right)\right] \tag{12}$$

So far we have considered amplification in a single slab. However, the output fluence from the first slab may be used as the input for a second pass or to the next slab, and so on, allowing in general different beam sizes and grazing angles to be considered for each stage of the amplifier chain.

2.3 Amplification in pulsed, high-frequency regime ($f \geq 1/\tau$)

This operating regime is mostly employed in laser systems for industrial applications, where high processing speed is generally required, even at the expense of some pulse energy reduction. In this case a cw pump laser is chosen owing to duty-cycle limitations of more powerful qcw laser diode arrays employed at lower frequency (typically < $1/\tau$). The amplifier gain (or the inversion population) between two amplified pulses is still restored according to Eq. (9), starting from the gain g_i just after the amplified pulse and reaching g_f just before the next seed pulse enters the amplifier. The Franz-Nodvik model can still be used, provided we use the right initial gain, which, in turns, depends on the pulse repetition frequency[10]:

$$F_o = F_S \ln\left[1 + \left(e^{F_i/F_S} - 1\right)e^{g_i}\right] \tag{13}$$

$$g_i = g_\infty - \left(g_\infty - g_f\right)e^{-\frac{1}{f\tau}} \tag{14}$$

$$F_o = F_i + \left(g_i - g_f\right)F_S \tag{15}$$

Following Koechner's notation, $g_\infty = \lim_{f\to 0} g_i(f)$ hence we identify $g_\infty = g_0$ as given in Eq. (11). Again, Eqs. (13-15) apply to single-pass amplification, but sequential application of the same model readily accounts for multi-pass schemes or amplifier chains. Note that this model is valid for any pulse repetition frequency, actually.

2.4 Bandwidth limitation and gain narrowing

The most important of limitations arising from the finite bandwidth of the amplifier concern single- or multi-pulse amplification in pulsed regime, when small-signal gain is very high, say > 1000. This situation is commonly encountered in regenerative and multi-pass amplifiers[13]. However, single-pass amplification in a couple of grazing-incidence Nd:YVO_4 slabs readily yields 60 dB overall small-signal gain, leading to severe pulse broadening if too short seed pulses are injected. In order to predict this effect quantitatively, we developed a numerical model based on Franz-Nodvik equations, adding gain filtering (of lorentzian form with fwhm = $\Delta\nu_g$) on each of the M slices into which the amplifier is sectioned. The basic assumption is that the gain depletion in each slice must be small enough (< 1%), so that we may apply the exact gain-filter model:

$$\hat{u}_{n+1}(\nu) = \hat{u}^{(u)}_{n+1}(\nu)\exp\left[\frac{\left(g_{n+1} + g_n\right)}{2}\frac{\gamma(\nu)}{2}\right] \tag{16}$$

$$\gamma(\nu) = \frac{1}{1 + \left(2\nu/\Delta\nu_g\right)^2} \tag{17}$$

$$u_n(t) = \int_{-\infty}^{+\infty} \hat{u}_n(\nu)e^{-i2\pi\nu t}\,d\nu \tag{18}$$

where $\hat{u}^{(u)}_{n+1}(\nu)$ is the Fourier transform of the amplified (unfiltered) field $u^{(u)}_{n+1}(t)$ at the end of the (n+1)-th section, according to the Franz-Nodvik model:

$$G_{n+1} = \frac{e^{E_n/E_S}}{e^{E_n/E_S} - 1 + 1/G_n^{(0)}} \tag{19}$$

$$E_n = \int_{-\infty}^{+\infty} \left| u_n^2(t) \right| dt \tag{20}$$

$$G_n^{(0)} = G_0^{1/M} \tag{21}$$

$$g_n = \ln\left(G_n\right) \tag{22}$$

Here G_0 is the total small-signal gain, and g_n is the result of the previous step. The condition for accurate computation is that

$$\frac{g_n - g_{n+1}}{g_n} \ll 1 \tag{23}$$

This criterion guides the choice of the minimum value of M. We notice that computation time might be conveniently reduced provided one chose a logarithmic distribution of amplifier sections lengths, since most severe saturation occurs at the end of the amplifier. However, in order to model amplifier gains as high as 60 dB, we found that M = 500 yields sufficiently accurate results with only few seconds of computation time on a 2.4-GHz laptop.

Let us consider typical data for a pulsed grazing-incidence Nd:YVO_4 amplifier: $\Delta\nu_g$ = 212 GHz (a-cut Nd:YVO_4, fluorescence fwhm = 0.8 nm) F_S = 125 mJ/cm^2 and E_S = 188 μJ. We calculated the output energy and pulse width as a function of small-signal gain, input energy and seed pulse width. The results are summarised in Fig. 2 and Fig. 3.

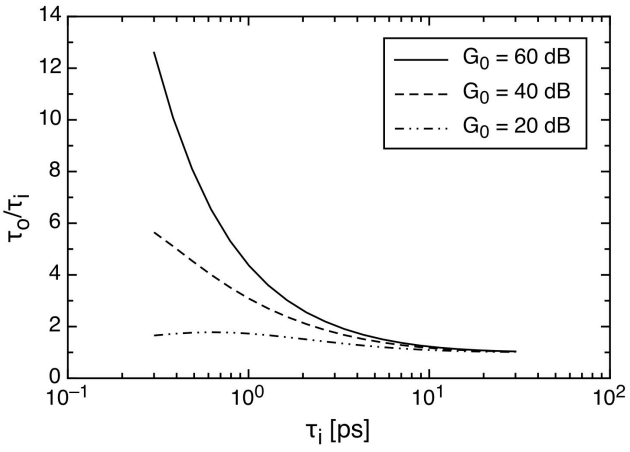

Figure 2. Output pulse width as a function of the seed pulse width, for three different value of G_0.

In conclusion, we note that seed pulse duration exceeding four times the minimum width set by the amplifier bandwidth (≈ 1.5 ps in this example, assuming *sech*^{2} pulse shape) produce no significant broadening after amplification even at an unsaturated gain of 60 dB (Fig. 2). The gain narrowing effect is most clearly seen at shorter seed pulse widths, as expected. Notice that at relatively low gain values, G_0 < 20 dB, the output pulse width reaches a maximum broadening as the seed pulse shortens, then approaches the seed duration provided it is short enough. The physical explanation is that the gain modulation is not as strong as with higher gain, so that only a relatively small central region of the seed spectrum is amplified but the overall non-amplified spectrum energy dominates, leading to an output pulse width still approaching that of the seed pulse.

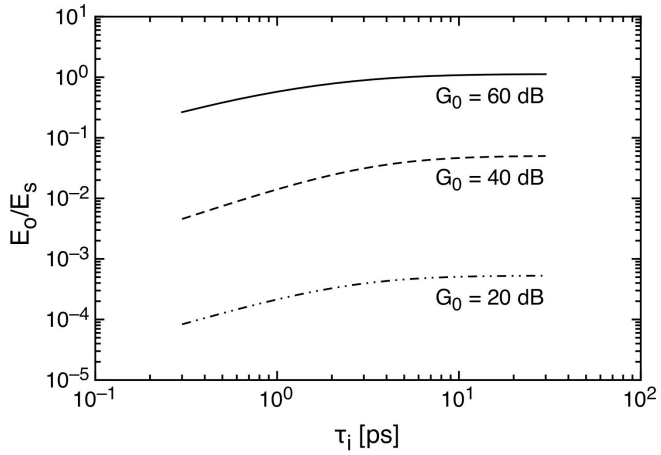

Figure 3. Output energy as a function of the seed pulse width, for three small-signal gain levels. Injected seed energy is 1 nJ.

As far as efficient energy extraction is of concern, Fig. 3 shows that with the given (typical) amplifier parameters a small-signal gain G_0 = 50-60 dB is required to reach saturation starting from the typical seed energy level ≈ 1 nJ. It is remarkable that, whilst this is usually achieved with either regenerative or extra-cavity multi-pass setups, typical gains of qcw grazing-incidence modules ≈ 30 dB/slab yield such gain levels with only two slabs or a single slab in two-passes, if only one is careful enough to suppress ASE.

2.5 Temporal distortions from amplifier saturation

This effect is most relevant when amplifying relatively long pulse trains, typically with an envelope duration > 50 ns for G_0 ~ 60-70 dB. It originates from the strong amplification experienced by the leading edge of the train envelope, which depletes the gain reducing the amplification of the trailing edge of the pulse. The distortion can be readily calculated from the Franz-Nodvik model, given the power envelope *P(t)* of the pulse train, the small-signal gain G_0 and the saturation energy E_S:

$$G(t) = \frac{e^{E_i(t)/E_S}}{e^{E_i(t)/E_S} - 1 + 1/G_0} \tag{24}$$

$$E_i(t) = \int_{-\infty}^{t} P(t')\,dt' \tag{25}$$

$$P_o(t) = G(t)P_i(t) \tag{26}$$

Therefore, the envelope modulation waveform required for pre-compensation of the saturation distortion can be easily computed, in order to yield a nearly flat-top output pulse from the amplifier. Owing to the strong amplifier saturation, the output energy reduction due to the pre-compensation is not very penalizing, notwithstanding the significant energy reduction of the modulated seed.

3. EXPERIMENTAL RESULTS

3.1 Amplification of a cw mode-locked picosecond laser

The simplest setup that one can conceive is a single grazing incidence slab, side-pumped by a single diode array, for amplification of a low-power cw picosecond laser. In our experiments the seeder is a Nd:YVO_4 oscillator longitudinally pumped by a 1-W laser diode at 808 nm. The laser is passively mode-locked with a SESAM. Since in our setup the output coupler is a folding mirror, there are two diffraction limited output beams each carrying 50-mW average power train of 6.8-ps, linearly polarized pulses at a 150-MHz repetition rate.

A 4 x 2 x 16 mm^3, *a*-cut, 6°-wedged, 1%-doped Nd:YVO_4 slab is employed as amplification head, pumped by a TE-polarized 10-mm x 1-µm laser diode array, emitting at 808 nm and collimated along the fast-axis by a 0.9-mm focal length microlens. This laser diode is actively cooled and temperature controlled with a thermoelectric cooler and its maximum output power is 32 W. The amplifier crystal is antireflection (AR) coated at 1064 nm on the input and output faces and simply polished and uncoated on the pumped side face. The Fresnel loss of about 14% of the incident pump power limits the absorbed pump power at 28 W. The 4 x 16 mm^2 slab faces are placed in contact with a water-cooled heat exchanger by thin indium foils. A proper choice of the water temperature set point is crucial in optimizing the amplifier performances, as this allows minimization of the thermal stress inside the slab and reduction of the thermal red-shift of the fluorescence bandwidth of Nd:YVO_4, that may reduce the amplifier gain and performance. In this case the optimum operating temperature is 8°C. The collimated beam emitted by the pump diode is polarization-rotated by a half-wave plate and focused into the Nd:YVO_4 slab with a 15-mm focal length cylindrical lens.

The setup for the cw amplification experiments is shown in Fig. 4.

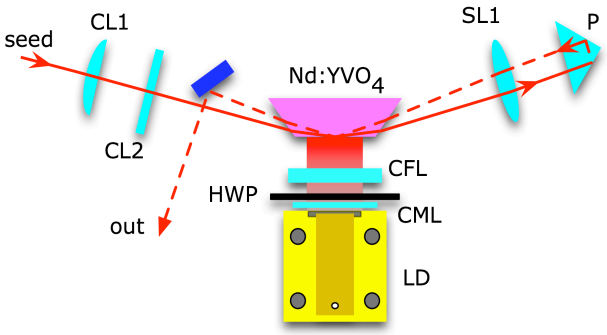

Figure 4. Setup for the cw amplifier. CL1: 250-mm focal cylindrical focusing lens; CL2: 100-mm focal cylindrical focusing lens; SL1: 200-mm focal spherical lens; P: right-angle prism; CFL: 15-mm focal cylindrical pump focusing lens; HWP: half-wave plate; CML: collimation microlens (0.9-mm focal length).

Being the thickness W of the gain sheet set by the pump focusing lens and limited by the residual smile of the laser diode, the depth of the gain sheet in the horizontal plane is basically determined by the pump absorption depth, $1/\alpha_P \approx$ 0.5 mm, given the typical pump spectrum width (≈ 2-3 nm) and the 1%-doping concentration of Nd:YVO_4. This generates an elliptical transverse gain profile that suggests the need for a different seed focusing in the horizontal and vertical directions. As shown in Fig. 4, the cylindrical lens CL1 focuses the oscillator beam down to $w_x \approx 100$ µm in the horizontal plane, whereas a cylindrical lens CL2 focuses the seed beam in the vertical plane to $w_y \approx 36$ µm. In order to choose the seed waist inside the amplifier, both the thickness of the pumped region and the Rayleigh range of the focused beam should be taken into account. In particular the pumped region length along the seed propagation direction should be shorter than the confocal parameter of the focused beam, in order to take advantage of the entire length of the active region. These considerations set a minimum acceptable dimension of ≈ 30 µm for the focused seed beam waist. Moreover, the grazing incidence angle has to be chosen as small as possible in order to maximize the gain while avoiding clipping effects.

With 34-mW seed injection the amplifier yields as much as 6.1 W after a single pass for the 28-W absorbed pump power, corresponding to a 22% optical-to-optical efficiency. The beam quality of the seed (M^2 = 1.1) is only slightly degraded to M_x^2 = 1.3 and M_y^2 = 1.3 at the maximum amplification level. The pulse duration after amplification is only slightly increased and the effect of spectral gain narrowing is quite evident. Starting from 6.8-ps long seed pulses we obtain 7.5-ps long amplified pulses, while the spectrum narrows from 0.38 nm down to 0.21 nm. We notice that, owing to dishomogeneous broadening due to spatial hole burning, longitudinally-pumped picosecond lasers with gain at the end usually show excess bandwidth with respect to the measured pulsewidth. Therefore, in this case gain narrowing improves the pulsewidth × bandwidth product from 0.68 for the seed to 0.42 for the amplified pulses measured after the second pass in the amplifier, approaching the Fourier limit of 0.32 for a $sech^2$ pulse shape.

Double-pass amplification can be conveniently realized by re-imaging the single-pass output with a spherical lens SL1 (200-mm focal length) and a right-angle antireflection-coated prism P (see Fig. 4), thus maintaining the same spot size as in the first pass, but with a slightly increased grazing angle of ≈ 4°. Beam extraction occurs before the lens CL2. The first

consequence of realizing a return path in the amplifier is the immediate growth of the amplified spontaneous emission (ASE) background. When the pump diode beam is focused for single-pass amplification, addition of the second pass boosts the ASE to > 1 W in this setup. In order to reduce the gain in the amplifier and hence the amount of ASE, the pump diode focusing must be relaxed, for example replacing the 15-mm cylindrical lens with a 20-mm lens. This increases W to ≈ 95 μm. In this way ASE background reduces to < 200 mW and as much as 8.4 W are obtained at 28-W absorbed pump power after 2nd pass amplification. The corresponding optical-to-optical efficiency increases to ≈ 30%.

Both in single or double pass setup, a small signal gain higher than 40 dB for the lowest input power is obtained. The model employed for fitting the experimental data is described in Section 2.1. The following physical parameters of the laser crystal can been used to fit the experimental data: $I_S = 2$ kW/cm^2, $\alpha_{P0} = 24$ cm^{-1}, $I_{SA} = 3.61$ kW/cm^2. The unsaturated absorption coefficient has been calculated assuming the absorption spectrum averaged over the laser diode emission spectrum. The best-fit saturation intensity value I_S yields a product στ about 30% smaller than the one usually reported in literature. Such a behavior, beside intrinsic model approximations, can be explained by a reduction of the fluorescence lifetime due to up-conversion effects and by a reduction of the effective emission cross section due to the mismatch between the spectrum peaks of seed and amplified pulses.

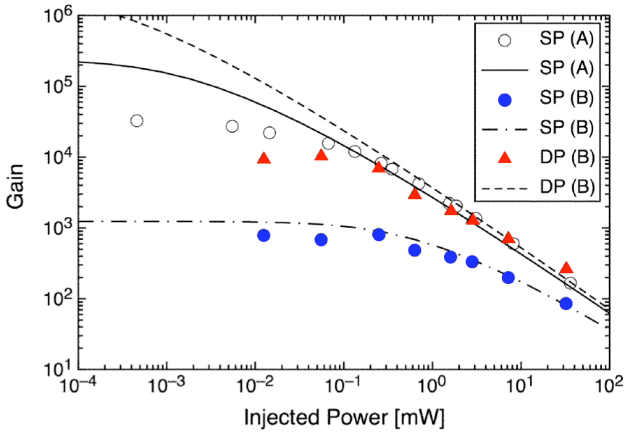

Figure 5. Gain curves for the single- and double-pass amplifier. (A) Setup with pump focusing with 15-mm focal and seed focusing with cylindrical lenses of focal lengths $f_x = 250$ mm and $f_y = 100$ mm. (B) Setup with pump focusing with 20-mm focal and seed focusing with 300-mm focal spherical lens. SP single pass, DP double pass. Continuous curves: numerical results. Points: data.

As clearly shown in Fig. 5, the amplifier behavior tends to deviate from the model for decreasing injected power levels, suggesting that the maximum available gain is lower than that predicted. For very small injected power, gain saturates around ≈ 10^4 owing to ASE, while gain saturation with higher input seed power levels recovers a fair agreement between predictions and experiments, since stored energy is more effectively extracted from the amplified beam rather than being wasted into wide-angle ASE.

3.2 Amplification of a multi-kHz PQS sub-nanosecond laser

In this experiment, the master oscillator is a PQS Cr^{4+}:YAG/Nd:YAG laser longitudinally pumped by a 40-W diode laser array driven at ≈ 40-μs 40-A current pulses, generating ≈ 60-μJ, <500-ps-long diffraction limited single longitudinal mode pulses at 10 kHz[14]. Owing to the good overlap between Nd:YAG and Nd:YVO_4 gain bandwidths, an *a*-cut 4 × 2 × 15 mm^3, 1% doped, 6° wedged vanadate slab is chosen for amplification. The end faces of the slab are antireflection-coated (AR) at 1064 nm while the pumped side is AR-coated at 808 nm. The slab is pumped by a 40-W cw diode laser array vertically polarized parallel to the slab's *c*-axis, tuned at 808 nm and collimated by a microlens CML (Fig. 6), yielding a gain sheet of ≈ 200 μm in the vertical direction. The depth of the gain sheet in the horizontal plane is basically determined by the pump absorption depth, $1/\alpha_P \approx 0.5$ mm, given the pump spectral width and the doping concentration of Nd:YVO_4. The 4 × 15 mm^2 faces are placed in contact, by thin indium foils, with a water-cooled heat exchanger. In order to optimize the energy extraction and to reduce the thermal aberrations, both the incidence angle and the seed beam waist inside the amplifier medium must be properly controlled. A good mode matching between injected seed and

elliptical cross section ≈ 0.5 × 0.2 mm^2 of the gain sheet is then required. As shown in Fig. 6, the spherical lens L2 (300-mm focal) focuses the seed beam in the slab to match the horizontal gain diameter, while a cylindrical lens CL (50-mm focal) provides additional focussing in the vertical plane. The grazing angle needs to be chosen as small as possible in order to both maximize gain and avoid clipping effects.

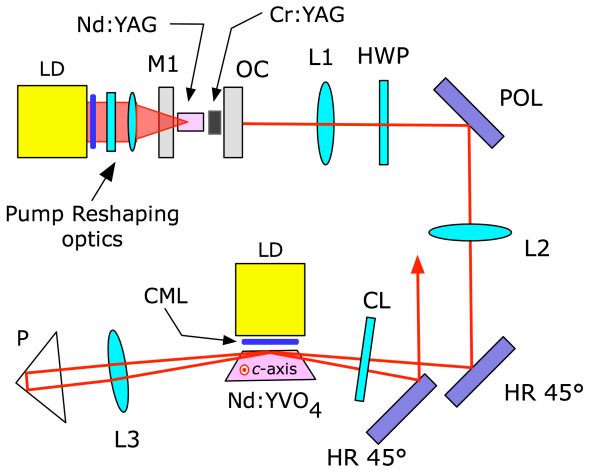

Figure 6. Laser setup. LDs: pump laser diodes (40-W linear arrays), fast-axis collimated with microlens (CML). The PQS oscillator includes the input mirror M1 (concave, r=1 m) and the 30%-reflectivity output coupler OC. L1: collimating lens (75-mm focal); HWP: λ/2 plate; POL: 45° polarizer; L2: 300-mm focal lens; CL: cylindrical lens (50-mm focal); L3: spherical lens (100-mm focal); P: right-angle prism. The Nd:YVO_4 slab is *a*-cut with vertical *c*-axis, parallel to pump diode polarization.

Double-pass amplification is realized by re-imaging the single-pass output with a spherical lens L3 (100-mm focal) and a right-angle AR-coated prism P, thus maintaining the same spot size as in the first pass, but with a slightly larger grazing angle. Beam extraction occurs after the lens CL.

As shown in Fig. 7, as much as 3.81 W in single-pass and 5.45 W in double-pass at 10 kHz are obtained at 38.4-W pump power, corresponding to an extraction efficiency ≈ 13% and energy per pulse of 381 and 545 μJ respectively.

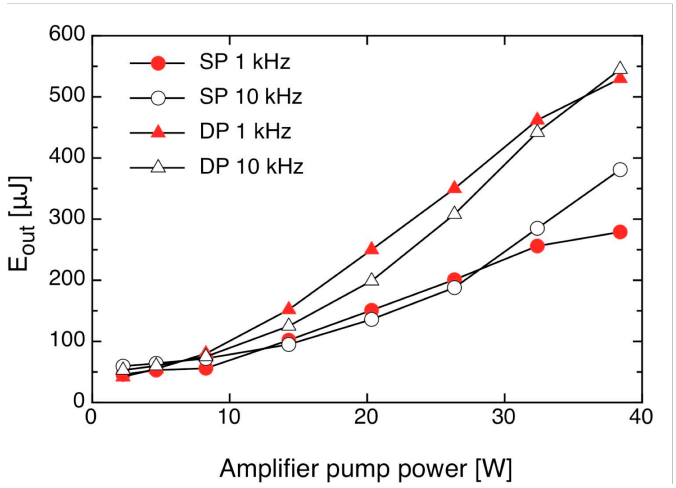

Figure 7. Single- and double-pass (SP, DP) output energy as a function of the pump power incident (and almost completely absorbed) on the Nd:YVO_4 slab amplifier.

Clearly, tighter focussing of the diode array into the slab readily increases the gain and would improve the performance accordingly, but one also needs to trade off amplifier efficiency with damage-free operation. In facts, the peak intensity

reaches 2 GW/cm^2, approaching the nominal damage threshold of the AR coatings at 1064 nm for 500 ps pulses (≈ 500 MW/cm^2 for 10 ns pulses). The beam quality of the MOPA system was measured with a CCD camera, with the amplifier either switched off ($M_x^2 \times M_y^2$=1.1 × 1.0) or switched on at full pump power ($M_x^2 \times M_y^2$ = 1.2 × 1.0). Only the two-pass result was measured, since this brings the stronger thermal aberration and beam quality deterioration. No significant worsening with respect to the TEM_{00} seeder profile is observed.

Both the average output power and the pulse energy are maximized at 10 kHz. Fig. 8 shows the gain and the output energy E_{out} at 10 kHz, as a function of the seed energy E_{in}, that is controlled by a variable attenuator. For better clarity we only report the gain curves of the double-pass setup. These curves have been fitted to the model described in Section 2.3 allowing determining the small-signal low-frequency exponential gain g_∞ and the saturation energy E_{sat}.

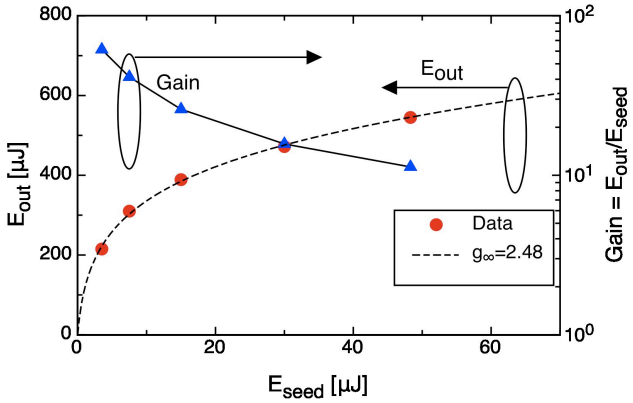

Figure 8. Double-pass gain and output energy as a function of the pump power incident (and almost completely absorbed) on the Nd:YVO_4 slab amplifier.

3.3 Single-pulse amplification up to 1 kHz repetition rate

A representative layout of a laser system for single picosecond pulse amplification after pulse-picking is shown in Fig. 9. The master oscillator in this case is still similar to that used for cw experiments, providing two output beams each carrying out about 70-mW average power, 7.7-ps long pulses but with a reduced repetition rate ≈ 48-MHz. This last parameter is important since well-separated pulses are easier to pick up with optoelectronic devices. The repetition frequency downscaling scheme for single pulse amplification employs an acousto-optic modulator (AOM) to pick up single pulses from the cw mode-locked oscillator. The major benefit of using AOM with respect to faster electro-optic modulators for pulse picking is the simpler and easier to customise driving electronics. Moreover AOMs are cheaper and do not require fast switching of high voltages that generates electromagnetic noise difficult to suppress. The pulse train sampled by the pulse picker has programmable repetition frequency, basically upper-limited by the duty cycle of the high-power diode arrays pumping the amplifier stage that is typically 10%. In case of vanadate slab amplifiers, since the fluorescence time is ≈ 100 μs, the maximum operating frequency for qcw laser diodes bars is fixed at 1 kHz.

The amplification stage setup is shown in detail in Fig. 10. The seed emerging from the pulse picker is injected into a grazing-incidence single-pass amplifier made by a couple of 4 × 2 × 16 mm^3, *a*-cut, 5°-wedged, 1%-doped Nd:YVO_4 slabs. The slabs are AR-coated at 1064 nm at the input and output faces, while the pumped sides are AR-coated at 808 nm. Each slab is pumped by a 150-W peak power qcw laser diode array with an emitting size of 10 mm × 1 μm. The radiation emitted by each diode is collimated by a microlens to ≈ 0.9-mm thickness × 10-mm width stripe and polarisation rotated by a half-wave plate to be aligned with the *c*-axis of the vanadate slabs. Notice that, owing to the much higher peak power of the diode arrays, tight focusing into the slab is no more required as in the cw amplifier of Section 3.1.

Pulse duration is slightly increased after energy amplification to 210 μJ. Fwhm 7.7-ps long seed pulses are slightly stretched to 11 ps long. The 0.37-nm wide pulse spectrum is substantially preserved during amplification, improving the quality parameter pulsewidth × bandwidth.

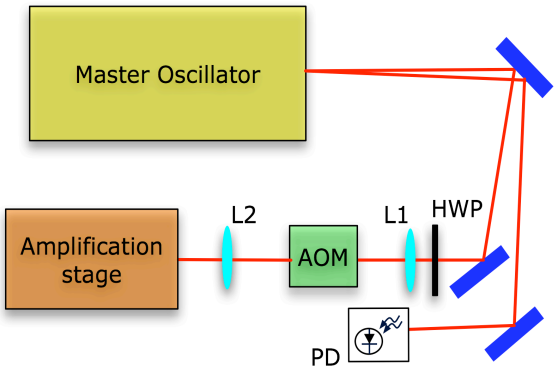

Figure 9. Layout of a laser system for single pulse amplification. HWP: half-wave plate; L1: focusing spherical lens; L2: collimating spherical lens; AOM: acousto-optic modulator; PD: photodiode.

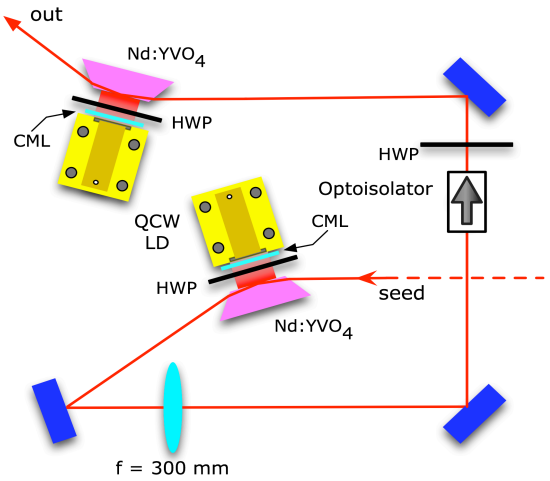

Figure 10. Setup for the single-pulse amplification 2-slabs module. HWP: half-wave plate; CML: collimation microlens (0.9-mm focal).

In order to fully exploit the potential of high-gain amplifier modules, besides the optimisations concerning the grazing angle as well as the matching between the seed beam waist and the gain layer, the main issue is to be able to contrast successfully those effects, such as amplified spontaneous emission (ASE), that compete with the amplifying beam in depleting the population inversion in the gain media. Since the ASE generated in the one slab can seed the other, the two amplifiers must be kept sufficiently separated, about 30 cm in this setup, in order to reduce the solid angle under which the first slab is seen by the second and consequently reduce the reciprocal ASE seeding. This solution yields significant performance improvements with respect to more closely separated slabs only few centimetres apart[15]. Furthermore, an opto-isolator is inserted between the two amplifiers to prevent self-oscillations and back-injection in the direction of the master oscillator. A spherical lens (300-mm focal length) placed at about 250 mm from the second slab re-collimates the spatial mode before entering the second amplifier.

The model for experimental data fitting is described in Section 2.2. The following best-fit parameters values are obtained: saturation fluence F_S = 133 mJ/cm^2 (correspondent effective emission cross-section $\sigma \approx 15 \times 10^{-19}$ cm^2), absorption coefficient α_P = 22 cm^{-1}, gain thickness W = 1.2 mm (flat-top approximation). For the seed beam it is assumed an equivalent flat-top profile diameter w_s = 0.6 and 0.8 mm in the first and second slab respectively, while the grazing

incidence angle θ is 1.6° in both slabs, according to a direct measurement of the deviation angle at the slabs output for the configuration yielding the highest pulse energy. Experimental results and relative model fitting are shown in Fig. 11.

Moreover, the numerical model suggests some useful optimisation criteria for further improvements of the system performances. First of all, in order to fully exploit the gain available in the first slab it is necessary to reduce the transverse dimensions of the seed beam in order to match its confocal parameter with the length of the pumped region. Such a relatively small beam size allows exploring smaller grazing incidence angles without clipping the beam, hence maximising the small-signal gain in the first unsaturated amplifier. Beam clipping should be carefully avoided, since it produces scattering and beam distortions that can substantially limit amplifiers performance. In the second slab the beam transverse dimensions and the grazing incidence angle should be increased in order to reduce non-linear effects and damage issues. The upper limit to input beam waist is given in this case by the gain region thickness W. According to this guidelines, output energy is predicted to increase up to 0.5 mJ with very small grazing incidence angles (≈ 0.3°) in the first slab and beam radius ≈ 0.5 mm in the second slab.

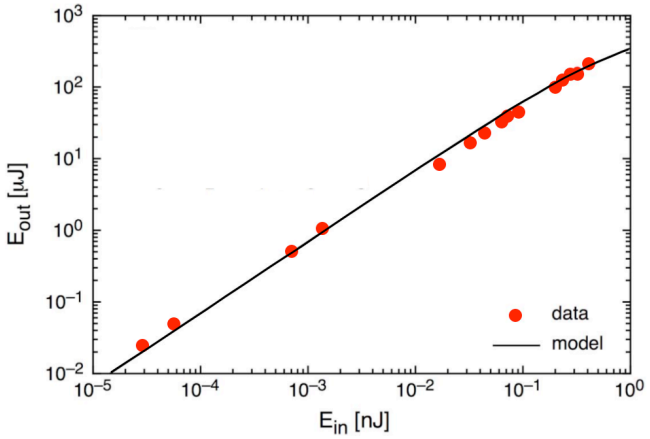

Figure 11. Amplifier energy extraction curve. Both experimental results and numerical model fitting are shown.

It is worth noticing that for an accurate measurement of the output pulse energy it is necessary to remove the contribution of both ASE and undesired background pulses. In fact, since the static extinction ratio of the AOM is ≈ 1:2000, this value can be considered the attenuation factor for pulses far away from the selected one, while pulses nearest to the selected one will surely experience an even lower extinction ratio. All of these contributions can become significant after amplification and affect a direct measurement carried out with a power meter. However, the post-amplification pulse contrast will be significantly increased by second harmonic generation (SHG), since the integrated contribution of the small background pulses will be practically negligible and the only significant contribution will come from the main pulse. Following these considerations, the amplified pulse energy at the fundamental wavelength can be inferred from a measurement of both SHG conversion efficiency and second harmonic pulse energy. This amplifiers yields as much as 160 μJ at 532 nm with a conversion efficiency of 75% in an angularly phase-matched 3 × 3 × 8 mm^3, type-I LiB_3O_5 (LBO) crystal without any focusing, owing to the high peak intensity level (≈ 4.8 GW/cm^2) of the nearly diffraction-limited amplified picosecond pulses. Fourth harmonic generation can also be readily performed, employing the SHG pulse as the pump for a 3 × 3 × 7 mm^3 β-BaB_2O_4 (BBO) crystal. As much as 64 μJ at 266 nm are generated with 40% conversion efficiency.

3.4 Amplification of high repetition rate pulse trains

Some applications require amplification of bunches of pulses instead of single pulses or continuous trains. The repetition rate of the micro-pulses contained in the bunches is set by the master oscillator, while temporal shape, duration and repetition frequency of the micro-pulses envelope (macro-pulse) can be settled by a suitable pulse-picking device. High small-signal single-pass gain diode side-pumped grazing incidence amplifier modules can be employed also for macro-pulse amplification, owing to their good performances in terms of gain, beam quality and micro-pulse duration preservation, their relatively simple optical arrangement and their cost effectiveness.

The main issue, peculiar of this application, is related to the severe temporal distortions experienced by the envelope of the macro-pulse during amplification, due to gain saturation and extremely high gain values. This effect is strongly dependent on the macro-pulse duration and in the end limits the possibility to obtain rectangular-shaped amplified envelopes for macro-pulses longer than few μs or even few hundreds of ns, depending on the amplifiers saturation level. In order to overcome amplification distortions it is necessary to inject in the amplifier chain a conveniently shaped macro-pulse with a temporal envelope designed to compensate saturation effects[16]. Modulating the radio-frequency driving signal of the AOM pulse picker can do this. An example of rectangular-shaped and custom-shaped macro-pulses is shown in Fig. 12.

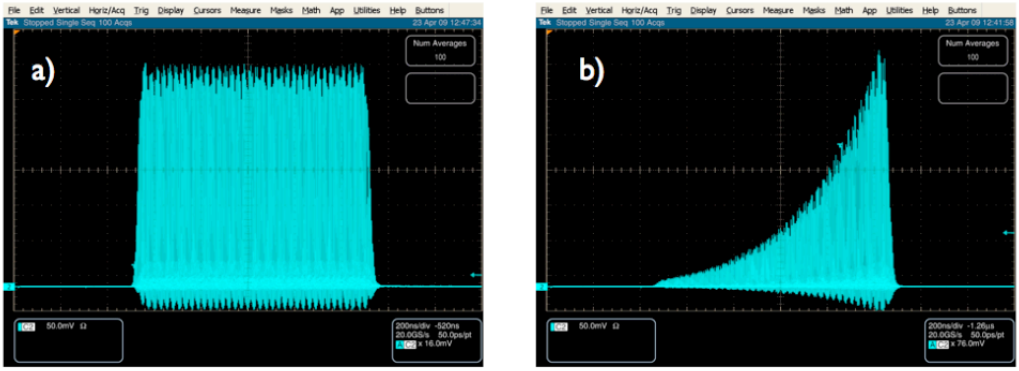

Figure 12. Examples of two different deflected waveforms. a) Rectangular-shaped macro-pulse envelope; b) Macro-pulse envelope reshaped for amplification distortions compensation. Note that the energy of the modulated envelope is reduced to ~ 1/3).

In the example reported here, the master oscillator for pulse train amplification experiments is a high-frequency passively mode-locked Nd:YVO_4 oscillator[17]. The ≈ 3-cm long V-folded resonator is pumped by a 1-W cw laser diode emitting at 808 nm, yielding ≈ 20-mW average power, ≈ 5-GHz repetition rate, 6-ps long mode-locking pulses. The AOM pulse-picker yields typically 500-ns long macro-pulses containing approximately 2500 picosecond micro-pulses from the continuous train (any macro-pulse length > 50 ns can be chosen). The macro-pulses are amplified employing three Nd:YVO_4 slabs, as shown in Fig. 13.

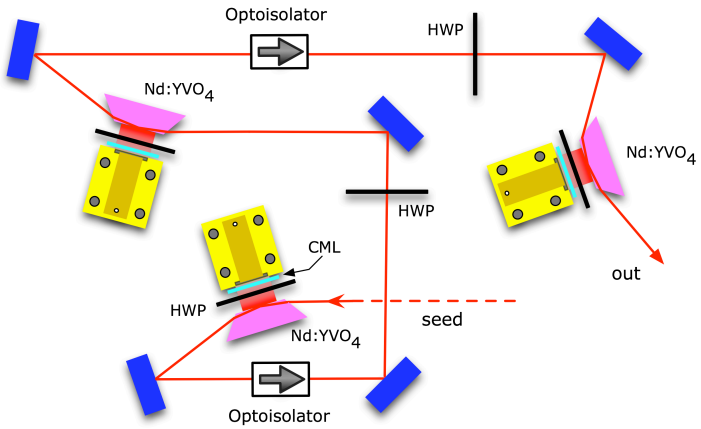

Figure 13. Diode pumped amplifiers setup for pulse train amplification. Each laser diode beam is polarisation-rotated by a half-wave plate (HWP) and collimated by a 0.9-mm collimation microlens (CML).

Each 14 × 4 × 2 mm^3, *a*-cut, 1% doped vanadate slab is side-pumped by a pulsed 150-W peak power laser diode array. A couple of opto-isolators are employed to prevent self-lasing and dangerous, high-intensity back-injections in the direction of the master oscillator. The deflected laser beam emerging from the AOM needs to be carefully collimated to a vertical dimension optimally matched to the pumped layer, while the path between the three amplification heads is kept sufficiently long in order to reduce the amount of ASE generated in the first amplifier and injected into the others. All

these optimisations contribute to achieve a single-pass gain of ≈ 70 dB. Pulse duration increases from 6 ps to 8.9 ps after amplification. Maximum output energy of about 2.5 mJ per macro-pulse is obtained after the three stage amplifier. The pulse spectrum after amplification is significantly narrowed: starting from a master oscillator 0.4-nm wide spectrum (fwhm), it shrinks to ≈ 0.19 nm at the output of the diode pumped amplifiers. Beam quality is well preserved ($M^2 \approx 1.2$) as Fig. 14 clearly suggests.

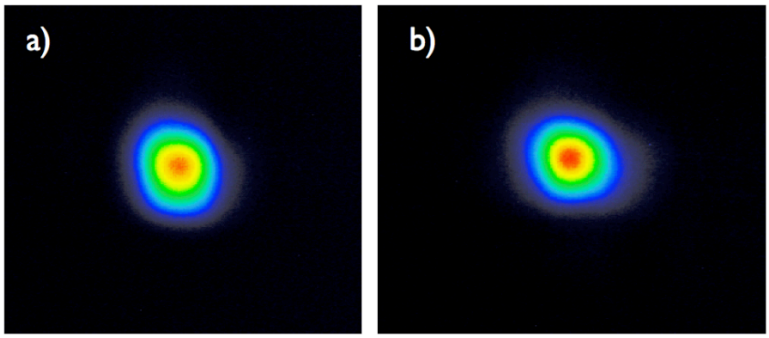

Figure 14. Laser beam profile before amplification (a) and at the amplifier output (b).

Macro-pulse repetition rates up to 1 kHz can be chosen, owing to the duty cycle limitation of qcw diode arrays discussed previously. A particular high-energy application that was subject of recent research requires a flash-lamp post-amplifier: the macro-pulses emerging from the diode pumped amplification stage are then further amplified in a couple of 12-cm long, 6-mm diameter, flash-lamp pumped Nd:YAG rods. At the maximum pump level, energy as high as 300 mJ is obtained for a 500-ns macro-pulse containing approximately 2500, 12-ps long micro-pulses. The good beam quality ($M^2 \approx 1.5$) and peak power > 10 MW of the single pulses in the amplified burst allows efficient nonlinear frequency conversion. SHG efficiency as high as 60% at 532 nm is achieved in a 16-mm long type-I LBO crystal. This second harmonic output beam is used to synchronously pump an optical parametric oscillator (OPO) plane-plane cavity. The nonlinear medium is a 12-mm long AR-coated KTP crystal cut for type II phase-matching. Both the OPO mirrors and the crystal coatings are designed for singly-resonant oscillation around 800 nm, even though much broader tuning behaviour might be obtained in principle, with a suitable choice of mirror coatings. At the maximum pump energy at 532 nm, with a 40% transmitting output coupler the OPO generates about 60 mJ at 800 nm, in 500-ns long, rectangular-shaped macro-pulses[19].

4. CONCLUSIONS

Effective amplification of diode-pumped picosecond laser oscillators employing grazing-incidence side-pumped slab modules has been presented. Numerical models, useful for the design and the investigation of the amplifier characteristics, both in terms of energy extraction and pulse dynamics, have been illustrated. Some particularly representative examples of such amplification techniques, under various operating regimes, have been reported and discussed, comparing their results with the numerical model. The most distinctive features of grazing-incidence amplifiers can be summarised as follows:

- extremely high gain that allows considerable setup simplification;
- strong gain shaping allowing beam quality preservation also along the fast axis of the diode array, notwithstanding the strong thermal lensing in that direction;
- compactness, modularity and easy scalability.

Higher power and energy levels can readily be obtained by adding pump diodes or even diode stacks, instead of using a single diode array to pump the bounce face of the slab[20].

Applications of this amplification technique can also be attractive for other laser materials such as Yb^{3+}-doped crystals (mostly Yb:YAG), Nd:glass, Nd:YAG and Nd:YLF. It is required that the absorption depth be small enough, and the absorbed pump power sufficiently high to produce a population inversion density yielding an integrated gain ≈ 20-30 dB per pass, in order to exploit all the useful features of the grazing-incidence slab. Particularly attractive are wide-band materials such as Nd:glasses that might allow high-energy femtosecond amplification with much simpler setups than

usually reported in literature, at least using powerful qcw diode arrays at relatively low frequency (< 1 kHz). Quasi-three level materials such as Yb^{3+}-doped crystals also allow sub-picosecond and femtosecond amplification, however their re-absorption losses have to be taken into account properly and the pump geometry carefully designed to maximise efficiency. On the other hand, they are definitely more attractive than glasses for power upscaling, owing to their superior thermal and mechanical properties.

Acknowledgments - This research received funding from the European Community's Seventh Framework Programme FP7/2007-2011 under grant agreement n◦224042.

REFERENCES

1. Dausinger, F., Hügel H. and Konov, V., "Micro-machining with ultrashort laser pulses: from basic understanding to technical applications," Proc. SPIE 5147, ALT'02 Int. Conf. Ad. Laser Tech., 106 (2003).
2. Breitling, D., Ruf A. and Dausinger F., "Fundamental aspects in machining of metals with short and ultrashort laser pulses," Proceedings of SPIE Vol. 5339 Photon processing in microelectronics and photonics III, 49 (2004).
3. McCarthy M. J. and Hanna D. C., "All-solid-state synchronously pumped optical parametric oscillator," Journal of the Optical Society of America B,10, 2180 (1993).
4. Sun Z., Ghotbi M. and Ebrahim-Zadeh M., "Widely tunable picosecond optical parametric generation and amplification in BiB3O6," Optics Express 15, 4139 (2007).
5. Mani A. A., Dreesel L., Hollander P., Humbert C., Caudano Y., Thiry P. A. and Peremans A., "Pumping picosecond optical parametric oscillators by a pulsed Nd:YAG laser mode locked using a nonlinear mirror," Applied Physics Letters 79, 1945 (2001).
6. Keller U., "Recent developments in compact ultrafast lasers," Nature 424, 831 (2003).
7. Neuhaus J., Kleinbauer J., Killi A., Weiler S., Sutter D. and Dekorsy T., "Passively mode-locked Yb:YAG thin-disk laser with pulse energies exceeding 13 μJ by use of an active multipass geometry," Optics Letters 33, 726 (2008).
8. Bernard J. E. and Alcock A. J., "High-efficiency diode-pumped Nd:YVO_4 slab laser," Optics Letters 18, 968 (1993).
9. Damzen M. J., Trew M., Rosas E. and Crofts G. J., "Continuous-wave Nd:YVO_4 grazing-incidence laser with 22.5 W output power and 64% conversion efficiency," Optics Communications 196, 237 (2001).
10. Koechner W., Solid-State Laser Engineering, Springer Berlin (2006).
11. Bermudez J. C. G., Pinto-Robledo V. J., Kir'yanov A.V. and Damzen M. J., "The thermo-lensing effect in a grazing incidence, diode-side-pumped Nd:YVO_4 laser," Optics Communications 210, 75 (2002).
12. Frantz L. M. and Nodvik J. S., "Theory of pulse propagation in a laser amplifier," Journal of Applied Physics 34, 2346 (1963).
13. Walker D. R., Flood C. J., van Driel H. M., Greiner U. J. and Klingerberg H. H., "High power diode-pumped Nd:YAG regenerative amplifier for picosecond pulses," Applied Physics Letters 65, 1992 (1994).
14. Agnesi A., Dallocchio P., Pirzio F. and Reali G., "Sub-nanosecond single-frequency 10-kHz diode-pumped MOPA laser," Appl. Phys. B (2009).
15. Agnesi A., Carrà L., Pirzio F., Reali G., Tomaselli A., Scarpa D., Vacchi C. and Braggio C., "High-gain diode-pumped amplifier for generation of microjoule-level picosecond pulses," Opt. Expr. 14, 9244 (2006).
16. Butterworth S. D., Clarkson W. A., Moore, N., Friel, G. J. and Hanna D. C., "High-power quasi-cw laser pulses via high-gain diode-pumped bulk amplifiers," Optics Comm. 131, 84 (1996).
17. Agnesi A., Carrà L., Pirzio F., Reali G., Tomaselli A., Scarpa D., Vacchi C. and Braggio C., "High-gain diode-pumped amplifier for generation of microjoule-level picosecond pulses," Opt. Expr. 14, 9244 (2006).
18. Agnesi A., Pirzio F., Reali G., Tomaselli A. and Braggio C., "Multi-GHz tunable-repetition-rate mode-locked Nd:GdVO4 laser," Opt. Express 13, 5302 (2005).
19. Agnesi A., Braggio C., Carrà C., Pirzio F., Lodo S., Messineo G., Scarpa D., Tomaselli A., Reali G. and Vacchi C., "Laser system generating 250-mJ bunches of 5-GHz repetition rate, 12-ps pulses," Opt. Express 16, 5811 (2008).
20. Minassian A., Thompson A., Smith, G. and Damzen M. J., "High-power scaling (>100 W) of a diode-pumped TEM00 Nd:$GdVO_4$ laser system," IEEE J. of Sel. Top. in QE 11, 621 (2005).